ELSEVIER

Chemical Engineering Science 60 (2005) 6169–6175

Chemical Engineering Science

www.elsevier.com/locate/ces

Numerical investigation of closures for interface forces acting on single air-bubbles in water using Volume of Fluid and Front Tracking models

W. Dijkhuizen, E.I.V. van den Hengel, N.G. Deen, M. van Sint Annaland*, J.A.M. Kuipers

Faculty of Science and Technology, University of Twente, P.O. Box 217, 7500AE Enschede, The Netherlands

Received 19 November 2004; received in revised form 31 March 2005; accepted 31 March 2005
Available online 25 May 2005

Abstract

Closures for the drag and virtual mass forces acting on a single air bubble rising in initially quiescent pure water have been numerically investigated using direct numerical simulation techniques. A 3D Front Tracking model was used and the results were compared with simulation results obtained with a 2D Volume of Fluid model to assess the influence of the third dimension. In the simulations realistic values were taken for the physical properties, i.e., a density ratio of 800. The computed time-averaged terminal rise velocity and mean aspect ratio for individual air bubbles ranging in equivalent diameter from 1 to 10 mm rising in pure water compare well with available experimental data.

Keywords: Front tracking; Volume of Fluid; Direct numerical simulation; Computational fluid dynamics; Gas–liquid flow

1. Introduction

Bubbly flows are widely encountered in industry as well as in everyday life. However, it has proved a daunting task to capture the behaviour of even single bubbles rising in an initially stagnant liquid in closure equations. Not only physical properties like density and viscosity of both phases and the surface tension strongly influence the behaviour of bubbles, but also the presence of infinitesimally small amounts of surface active molecules (Clift et al., 1978) or even the initial shape of the bubbles affect the bubble behaviour (Wu and Gharib, 2002; Tomiyama et al., 2002).

The difficulties in the description of the bubble behaviour arise to a large extent from the complex bubble shape deformation and bubble shape dynamics. Based on detailed experiments researchers (a.o. Tomiyama et al., 2002) have tried to capture the bubble shape with an ellipse, approximating the true interface shape dynamics.

However, with computational fluid dynamics the bubble shape and interface dynamics and their influence on the bubble behaviour can be studied in great detail. In this study direct numerical simulations (DNS) have been used to study the behaviour of a single air bubble rising in initially quiescent pure water, in order to derive closures for the drag and virtual mass forces acting on a bubble.

A full 3D Front Tracking (FT) model was used to calculate directly the drag and virtual mass forces. To assess the influence of the third dimension, these results were compared with the simulation results from a 2D Volume of Fluid (VOF) model. In all these simulations realistic values for the physical properties were used, i.e., a density ratio of 800. Moreover, experiments have shown a sharp decrease in the drag force coefficient for very small bubble diameters in the order of 1 mm. It has proven particularly difficult to simulate an air bubble in water of 1 mm diameter with VOF or FT models, due to parasitic currents or unacceptable volume losses caused by the surface tension treatment (Scardovelli and Zaleski, 1999). However with proper modifications regarding the implementation of the VOF and FT models, our codes could simulate these very small bubbles without

* Corresponding author. Tel.: +31 53 4894478; fax: +31 53 4892882.
E-mail addresses: w.dijkhuizen@utwente.nl (W. Dijkhuizen), M.vanSintAnnaland@utwente.nl (M. van Sint Annaland).

0009-2509/$ - see front matter © 2005 Elsevier Ltd. All rights reserved.
doi:10.1016/j.ces.2005.03.048

numerical problems. To the authors' knowledge this is the first time that simulation results are published for small bubbles (~ 1 mm) using actual physical properties.

2. Volume of Fluid and Front Tracking models

2D VOF and a 3D Front Tracking model were used to study the behaviour of a single bubble. In both models the incompressible Navier–Stokes equations were solved on a staggered Cartesian mesh using a two-step projection–correction method to obtain the pressure and flow field. In the FT model the interface consists of a number of interconnected triangular segments of which the forming points (vertices) are translated with the locally interpolated fluid velocity (Unverdi and Tryggvason, 1992; Tryggvason et al., 2001). In the VOF model (Delnoij, 1998) the interface is reconstructed for each computational cell with a piece-wise linear interface approximation. Using the orientation of the reconstructed interface the material fluxes through the cell faces are subsequently computed using geometrical advection.

The 3D FT model calculates the surface tension force acting on a triangular interface marker directly from the tensile forces due to its neighbours (van Sint Annaland et al., 2003). A higher order velocity divergence scheme, following Peskin and Printz (1993), has been implemented in the FT model, which made it possible to simulate bubbles smaller than 3 mm diameter without appreciable volume losses.

In the 2D VOF model the calculation of the surface tension was carried out with a similar tensile force as used in the FT model instead of the frequently used continuum surface force model (Deen et al., 2004), which significantly decreased the parasitic currents.

Since both the FT and VOF model do not contain any unclosed terms, all the closure equations for the forces acting on a bubble can be directly computed, which can subsequently be implemented in Euler–Lagrange or Euler–Euler models.

3. Derivation of closures for the forces from DNS simulations

The drag and virtual mass forces can be obtained from a simulation where a bubble is released in an initially stagnant liquid. From a steady state force balance in the vertical direction the stationary drag force coefficient C_D can be computed from the terminal rise velocity V_T (notation explained in the list of symbols):

$$C_D = \frac{4}{3}\frac{(\rho_l - \rho_g)|g|d_e}{\rho_l V_T^2}. \tag{1}$$

The virtual mass force coefficient can be computed from the initial part of the same simulation. Since the initial bubble rise velocity $w_{b,z}$ is negligibly small, only buoyancy and virtual mass forces are important. An instationary force balance yields the following expression for the virtual mass coefficient:

$$C_{VM} = -\frac{\rho_g}{\rho_l} + \frac{(\rho_l - \rho_g)|g|}{\rho_l \frac{\mathrm{d}w_{b,z}}{\mathrm{d}t}}. \tag{2}$$

4. Simulation details

The 2D VOF and 3D FT models were used to simulate initially spherical air bubbles rising in initially quiescent water with diameters ranging from 1 to 10 mm. With the 3D-FT model bubbles with a diameter larger than 7 mm oscillate so violently that the simulation eventually stops. The reason for this is too fast deformation of the surface mesh and consequently these problems are not encountered in the 2D VOF model. This might indicate break-up of the bubble, which is however not implemented in our present version of the Front Tracking model.

Further simulation details for both models have been summarised in Table 1. The typical wall time of a 3D FT simulation is about 2 months. For the 2D VOF simulations the bubbles were initially positioned one diameter above the bottom of the simulation domain. In the 3D FT model the more efficient moving window concept (with free-slip boundaries) is used, so that the centre of the bubble remained at $\frac{2}{3}$ of the height of the smaller computational domain. Whenever the bubble is more than one grid cell away from this specified position, the domain is shifted 1 cell accordingly. It was confirmed that the grid size was sufficiently small.

5. Results for the drag force

Firstly the computed time-averaged rise velocities have been compared with experimental data reported by Tomiyama (1998) and Grace et al. (1976). Tomiyama has reported drag relations for both contaminated and pure water and the corresponding terminal velocities have been plotted in Fig. 1. It must be noted here that there is a large scatter in the experimentally determined bubble rise velocities, which is indicated by the area surrounded by the indicated lines. Also the experimental correlation by Grace et al. has been included, which is valid for contaminated water only and starts to differ from the pure water data for bubbles at a bubble diameter below 3 mm. The differences between bubble rise velocities in pure and contaminated water have been attributed to the presence of surfactants, lowering the surface tension forces (Clift et al., 1978). However, Wu and Gharib (2002) and Tomiyama et al. (2002) independently pointed out a possible second cause: differences in the initial shape of the bubble, where a high initial deformation results in a high terminal rise velocity.

Table 1
Data used for the simulations to calculate the drag and virtual mass force coefficients for air bubbles rising in water

		Volume of fluid	Front tracking	Units
Dispersed phase	Density ρ_g	1.25	1.25	kg/m^3
	Viscosity μ_g	1.8×10^{-5}	1.8×10^{-5}	kg/(m s)
Continuous phase	Density ρ_l	1000	1000	kg/m^3
	Viscosity μ_l	0.001	0.001	kg/(m s)
	Surface tension σ	0.073	0.073	N/m
General	Morton number	2.52×10^{-11}	2.52×10^{-11}	—
	Grid size	160×320	$80 \times 80 \times 80$	—
	No. of cells equal to d_e	16	20	—
	Time step	1.0×10^{-5}	1 mm: 2.0×10^{-6} 2 mm: 5.0×10^{-6} Other: 1.0×10^{-5}	s

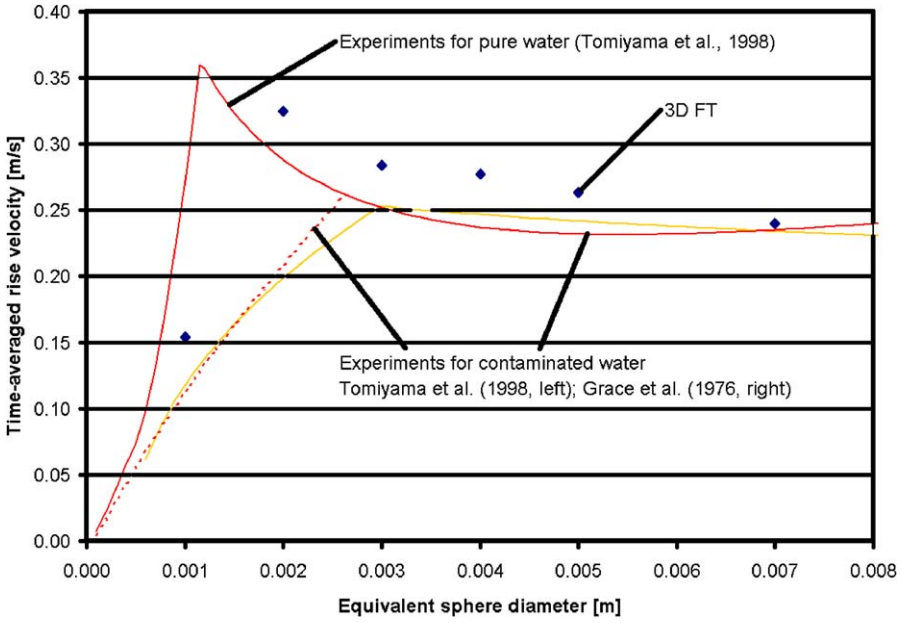

Fig. 1. Comparison of the computed time-averaged terminal rise velocity for air bubbles in water using the 2D VOF and 3D FT models with experimental data (Tomiyama et al., 2002; Grace et al., 1976).

The calculated terminal bubble rise velocities by the 3D FT model are quite close to the correlation by Tomiyama (1998). Note that they are time-averaged only for large bubbles, because of the shape oscillations. The slightly higher computed bubble rise velocities could even be attributed to the effects of infinitesimally small amounts of impurities in the 'pure' water used in the experiments.

Furthermore, it can be seen that the results of the VOF model correspond well with the experimental data for bubbles larger than 3 mm. However, large discrepancies can be discerned for smaller bubbles, due to the underestimation of the surface tension forces in a 2D model.

For the 3D FT model the instantaneous bubble rise velocity is given in Fig. 2. This figure clearly shows that the vertical velocity of air bubbles larger than 3 mm start to oscillate significantly. The air bubble with an equivalent bubble diameter of 7 mm even exhibits complex 3D oscillatory shape deformations. The initial acceleration of the bubbles however is the same.

In Fig. 3 snapshots of the computed bubble shapes are given, showing that the computed shape of the 1, 2, 3 and 7 mm bubbles is consistent for both simulation models. Fig. 4 shows the evolution of the aspect ratio (height divided by width) of the bubbles in time. From the 3D results, it can be seen that bubbles with an equivalent diameter of 5 mm and larger oscillate significantly and that the 7 mm bubble even has an asymmetrical oscillation in the x- and y-direction. In contrast 2D VOF

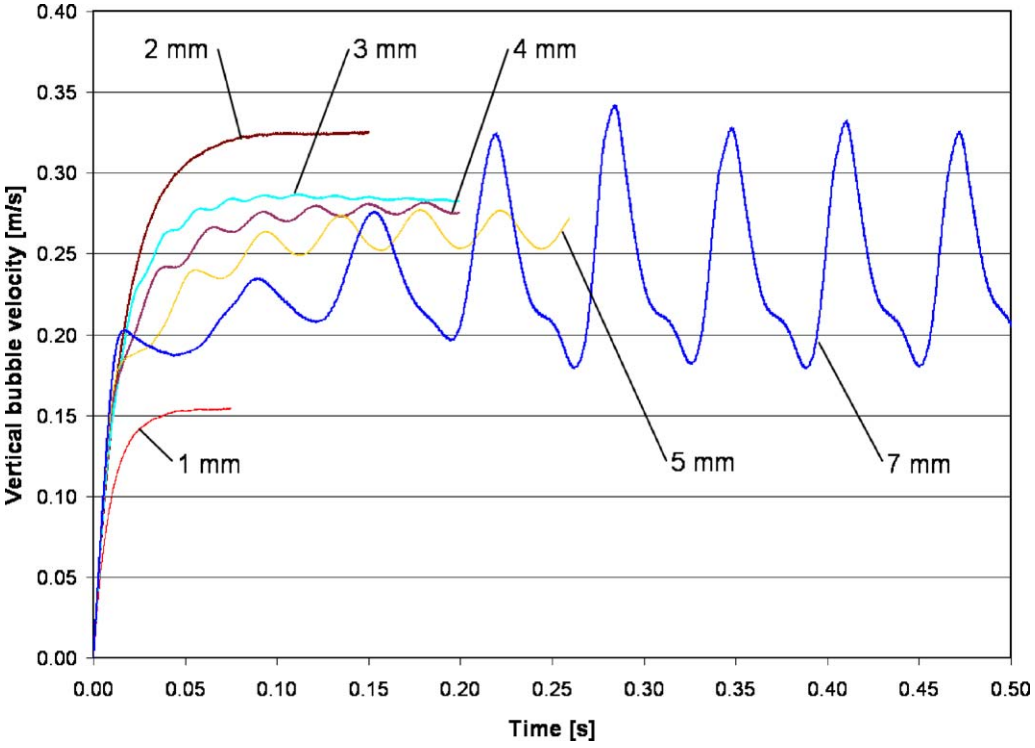

Fig. 2. Evolution of the vertical bubble velocity in time for bubbles with a different equivalent bubble diameter, computed with the 3D FT model.

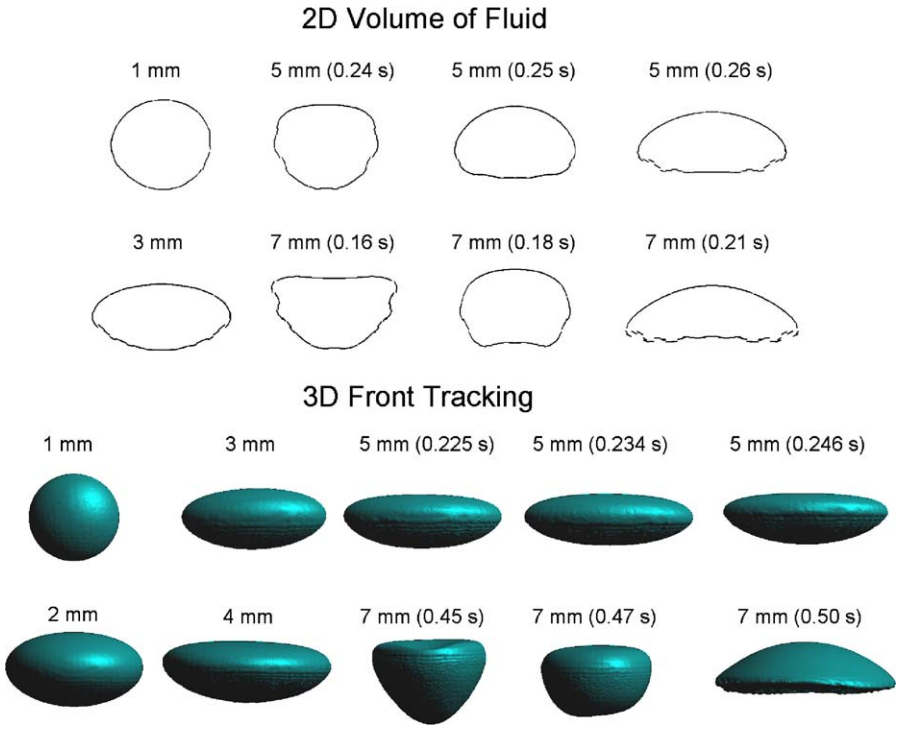

Fig. 3. Snapshots of the gas–liquid interface computed with the 2D VOF and 3D FT models for different equivalent diameters.

predicts oscillations for bubbles of 3 mm and larger and also the 1 mm bubble is more flattened than in the 3D simulations.

Tomiyama et al. (2002) derived the following equation for the terminal rise velocity of a bubble in the surface tension dominant regime, based on the potential flow theory, taking

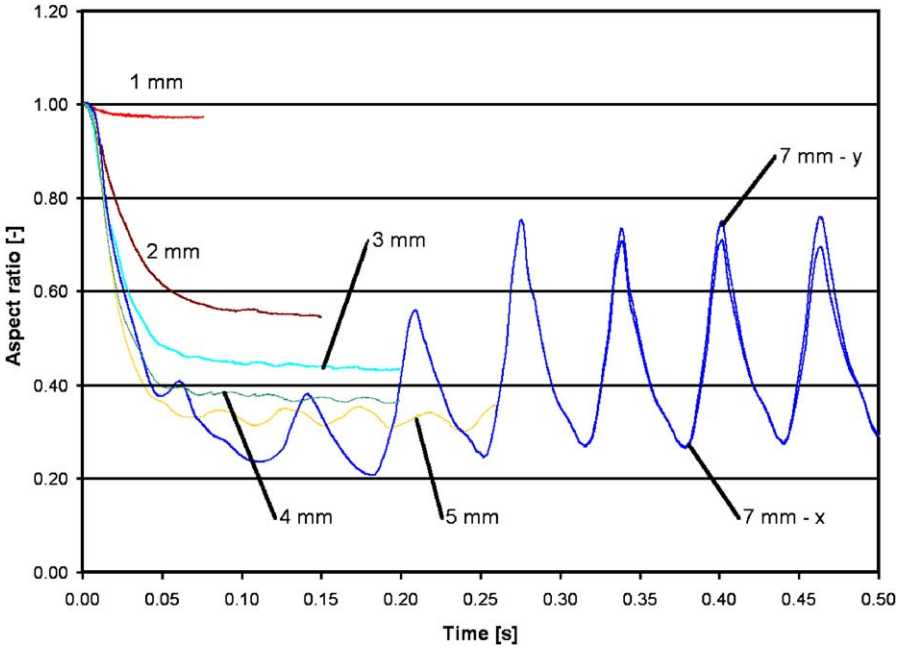

Fig. 4. Computed aspect ratio in time for bubbles with different equivalent bubble diameter; 2D VOF (left) and 3D FT (right).

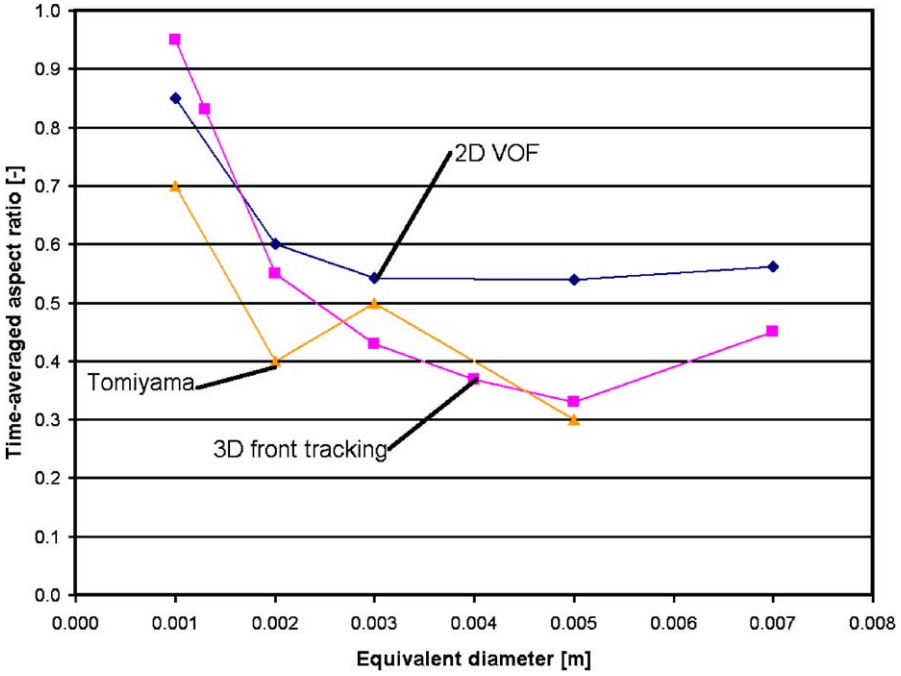

Fig. 5. Computed mean aspect ratio as a function of bubble diameter compared with experimental data by Tomiyama et al. (2002).

into account not only the equivalent diameter of the bubble, but also its mean aspect ratio:

$$V_T = \frac{\sin^{-1}\sqrt{1-E^2} - E\sqrt{1-E^2}}{1-E^2} \times \sqrt{\frac{8\sigma}{\rho_l d_e}E^{4/3} + \frac{(\rho_l-\rho_g)gd_e}{2\rho_l}\frac{E^{2/3}}{1-E^2}}. \quad (3)$$

They showed that their correlation corresponds very well with experimental data for air bubbles in pure water with an equivalent diameter in the range of 1.5–5 mm. Note that these experimental bubbles also exhibit shape oscillations, which are coupled to zigzagging or helical paths.

By coupling the equation for the terminal rise velocity with the drag correlation for pure water proposed by Tomiyama (1998), the mean aspect ratio can be deduced,

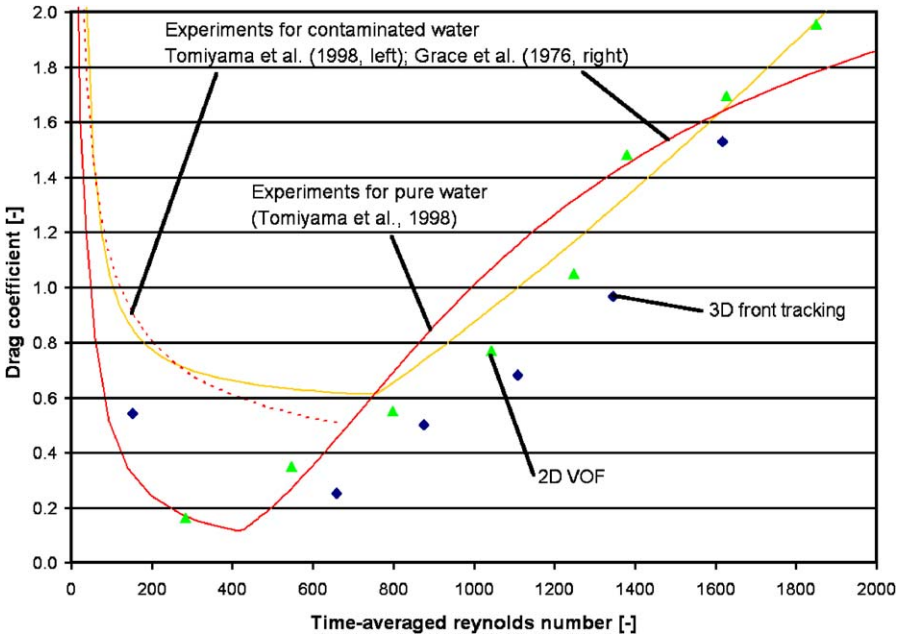

Fig. 6. Comparison of the computed drag coefficient as a function of the Reynolds number by the 2D VOF and 3D FT models with experimental data provided by Tomiyama (1998) and Grace et al. (1976).

and can be compared with the computed time-averaged aspect ratio (see Fig. 5). The predictions by the 3D FT model for the mean aspect ratio are quite good, while the 2D VOF model largely overestimates the mean aspect ratio for larger bubbles. The differences between the 3D model and the experiments can be attributed to the inherent shape deformation of bubble injection and the impurities still present in the distilled water used for the experiments.

Finally, the average rise velocity of the bubbles was used to calculate the drag force coefficients (Fig. 6). Both the 2D VOF and the 3D FT compare reasonably well with the experimental data. Somewhat smaller drag coefficients were computed, corresponding to the slightly higher computed terminal rise velocities.

6. Results for the virtual mass force

Results for the first millisecond after releasing an initially spherical bubble in quiescent water was used to calculate the virtual mass force coefficient, well before the bubble starts to deform (Table 2). With the 2D VOF model a virtual mass force coefficient of about 1.1 was determined, which agrees well with the literature (Auton, 1983; Lamb, 1932). With the 3D FT model a value only slightly higher than $\frac{1}{2}$, the theoretical value (Magnaudet and Eames, 2000), was found. With simulations using different initial bubble shapes the effect of the bubble shape on the virtual mass force coefficient can be studied.

Table 2
Computed virtual mass coefficients by the 2D VOF and 3D FT models for spherical bubbles of different sizes

Bubble diameter (m)	Virtual mass coefficient	
	2D VOF	3D FT
0.001	1.3	0.51
0.002	1.3	0.54
0.003	1.3	0.54
0.004	1.2	0.54
0.005	1.1	0.53
0.006	1.1	0.53
0.007	1.1	0.53
0.008	1.0	0.53
0.009	1.0	0.53
0.010	1.0	0.53
Theoretical value	1.0	0.50

7. Conclusions

A 3D FT and a 2D VOF model were used to numerically investigate the closures for the drag and virtual mass forces acting on a single air bubble rising in initially quiescent pure water. Air bubbles with an equivalent bubble diameter as small as 1 mm could be simulated without numerical problems due to parasitic currents or unacceptable volume changes using realistic values for the physical properties, i.e., a density ratio of approximately 1000. The computed time-averaged terminal rise velocity and mean aspect ratio for individual air bubbles ranging in equivalent diameter from 1 to 10 mm rising in pure water compare well with available experimental data for pure water systems. The

experimentally observed sharp reduction in the drag coefficient for air bubbles in water with an equivalent bubble diameter smaller than approximately 3 mm due to the increasing importance of the surface tension forces could be well reproduced with the 3D FT model, contrary to the 2D VOF model. A slightly higher terminal bubble rise velocity was computed by the models (with a corresponding lower drag coefficient) compared to the experimental data, which may be explained by an infinitesimal amount of impurities in the water used in the experiments. Furthermore, also the computed virtual mass coefficients correspond very well to theoretical predictions. Future work will be focussed on deriving closures for the lift force and the effects of shape deformation. Also swarm effects and the interaction between different dispersed phases will be investigated.

Notation

C_D	drag force coefficient, dimensionless
C_{VM}	virtual mass force coefficient, dimensionless
d_e	sphere-equivalent bubble diameter, m
E	aspect ratio (bubble height/width), dimensionless
g	gravitational acceleration, $\mathrm{m\,s^{-2}}$
Re	Reynolds number, dimensionless
V_T	terminal rise velocity, $\mathrm{m\,s^{-1}}$
w_b	bubble velocity relative to liquid, $\mathrm{m\,s^{-1}}$

Greek letters

ρ	density, $\mathrm{kg\,m^{-3}}$
σ	surface tension, $\mathrm{N\,m^{-1}}$

Subscripts

g	gas phase
l	liquid phase
z	Z-coordinate (opposite to gravity), m

Acknowledgements

This work is part of the research programme of the Stichting voor Fundamenteel Onderzoek der Materie (FOM), financially supported by the Nederlandse Organisatie voor Wetenschappelijk Onderzoek (NWO) and Shell Global Solutions.

References

Auton, T.R., 1983. The dynamics of bubbles, drops and particles in motion of liquids. Ph.D. Thesis, University of Cambridge, Cambridge, United Kingdom.

Clift, R., Grace, J., Weber, M.E., 1978. Bubbles, Drops and Particles. Academic Press, New York, pp. 169–202.

Deen, N.G., van Sint Annaland, M., Kuipers, J.A.M., 2004. Multi-scale modeling of dispersed gas–liquid two-phase flow. Chemical Engineering Science 59, 1853–1861.

Delnoij, E., 1998. Numerical simulation of bubble coalescence using a volume-of-fluid (VOF) model. International Conference on Multiphase Flow, ICMF'98 Proceedings, Lyon, France.

Grace, J.R., Wairegi, T., Nguyen, T.H., 1976. Shapes and velocities of single drops and bubbles moving freely through immiscible liquids. Transactions of the Institution of Chemical Engineers 54, 167–173.

Lamb, H., 1932. Hydrodynamics. sixth ed. Cambridge University Press, London.

Magnaudet, J., Eames, I., 2000. The motion of high-Reynolds number bubbles in inhomogeneous flows. Annual Review of Fluid Mechanics 32, 659–708.

Peskin, C.S., Printz, B.F., 1993. Improved volume conservation in the computation of flows with immersed elastic boundaries. Journal of Computational Physics 105, 33–46.

Scardovelli, R., Zaleski, S., 1999. Direct numerical simulation of free-surface and interfacial flow. Annual Review Fluid Mechanics 31, 567–603.

Tomiyama, A., 1998. Struggle with computational bubble dynamics. Third International Conference on Multiphase Flow, ICMF'98 Proceedings, Lyon, France.

Tomiyama, A., Celata, G.P., Hosokawa, S., Yoshida, S., 2002. Terminal velocity of single bubbles in surface tension force dominant regime. International Journal of Multiphase Flow 28, 1497–1520.

Tryggvason, G., Bunner, B., Esmaeeli, A., Juric, D., Al-rawahi, N., Tauber, W., Han, J., Nas, S., Jan, Y.-J., 2001. A front-tracking method for the computations of multiphase flow. Journal of Computational Physics 169, 708–759.

Unverdi, S.O., Tryggvason, G., 1992. A front-tracking method for viscous, incompressible, multi-fluid flows. Journal of Computational Physics 100, 25–37.

van Sint Annaland, M., Deen, N.G., Kuipers, J.A.M., 2003. Multi-level modelling of dispersed gas–liquid two-phase flows. Series: heat and mass transfer. In: Sommerfeld, M., Mewes, D. (Eds.), Springer, Berlin, pp. 139–157.

Wu, M., Gharib, M., 2002. Experimental studies on the shape and path of small air bubbles rising in clean water. Physics of Fluids 14, L49–52.